Extension of 1D linear stability analysis based on the Bridgman assumption. Applications to the dynamic stretching of a plate and expansion of a ring

M. Xavier, Sébastien Mercier, C. Czarnota, S. El Mai, D. Jouve, J.L. L Dequiedt, A. Molinari

Extension of 1D linear stability analysis based on the Bridgman assumption. Applications to the dynamic stretching of a plate and expansion of a ring.

M. Xavier[a,*], S. Mercier[b], C. Czarnota[b], S. El Mai[c],
D. Jouve[a], J.L. Dequiedt[a], A. Molinari[b]

[a] CEA, DAM, DIF, 91297 Arpajon - FRANCE
[b] Université de Lorraine -CNRS - Arts et Métiers ParisTech, Laboratoire d'Etude des Microstructures et de Mécanique des Matériaux, 7 rue Felix Savart, 57070 METZ - FRANCE
[c] CEA DAM, Gramat, 46500 Gramat - FRANCE

Abstract

The analysis of multiple necking phenomenon during dynamic stretching of a metallic plate is investigated. For that purpose, a new 1D linear stability analyses is proposed to capture the perturbation evolution. The multidimensional aspect of the stress field within the neck region is taken into account with a Bridgman correction factor. The novelty of the 1D approach is to let the time evolution of the perturbation determined by the linearized field equations. So, no predefined time dependency is assumed as in classical 1D linear stability analysis of the literature, see Zhou et al., An elastic-visco-plastic analysis of ductile expanding ring, Int. J. Impact Eng., 2006. The proposed model, named hereafter 1D-XLSA (standing for 1D-eXtended Linear Stability Analysis), can also be viewed as the restriction to 1D of the 2D-XLSA model developed in Xavier et al., Extension of linear stability analysis for the dynamic stretching of plates: Spatio-temporal evolution of the perturbation, European Journal of Mechanics-A/Solids, 2020. A comparison for a thermo-viscoplastic material with strain hardening is proposed for three possible routes : a 1D model based on the frozen coefficient theory named 1D-CLSA (standing for 1D-Classical Linear Stability Analysis), the proposed 1D-XLSA and 2D-XLSA models. It is shown that while growth rates in late deformation stage are similar, a strong difference in amplitude exists due to large discrepancies in the early deformation stage. The comparison also illustrates the importance of the modeling of multiaxiality of the stress field within the neck region and of initial defects. While differences between models are limited for perturbations with small wavenumbers, large discrepancies are observed for perturbations with large wavenumbers. Our model is also derived for the case of the extension of a cylindrical bar which is representative of the ring expansion during dynamic loading.

Keywords: Dynamic necking, Bridgman correction factor, Instability, Stability analysis, Ring, Plate

This is a post-peer-review, pre-copyedit version of an article published in International Journal of Solids and Structures. The final authenticated version is available online at: https://doi.org/10.1016/j.ijsolstr.2020.12.016.

*Corresponding author, e-mail: mathieu.xavier@cea.fr

1 Introduction

Fragmentation of ductile metals subject to dynamic expansion is a topic of interest for both civil and defense industries. The characterization of the fragment size distribution is one of the main concern since the kinetic energy is related to the size and velocity of fragments. The fracture process in ductile materials may be triggered by instabilities within the plastic flow that result in necking *i.e.* the occurrence of local thinnings where the plastic deformation is localized. When the structure expands at high-strain rates, multiple necks develop until failure resulting in multiple fragments.

Numerous experimental works using electromagnetical or explosive loadings have been conducted to understand the process of localization; various geometries were studied such as cylinders (see Wesenberg and Sagartz (1977), Olive et al. (1979), Fyfe and Rajendran (1980) or Goto et al. (2008)), rings (see Niordson (1965), Llorca and Juanicotena (1997), Zhang and Ravi-Chandar (2006)) or hemispherical shells (see Mercier et al. (2010)). From all experiments, it can be infered that the fracture process is divided in three steps (see Zhang and Ravi-Chandar (2006) for high-quality images): homogeneous deformation, development of local thinnings, fracture at some neck sites.

Analytical models have been developed in the last half-century to predict the fragment size distribution observed in experimental works. Pioneering work of Mott (1947) used a probabilistic approach and accounted for the stress release wave propagation within a metallic ring. While instantaneous fracture was postulated in Mott theory, Grady (1981) enriched it by accounting for the fracture energy dissipation and obtained results in agreement with experimental observations of Wesenberg and Sagartz (1977).

Bifurcation and linear stability analyses have been widely used in the last decades to tackle the issue of predicting necking by focusing on the early stages of the deformation. One may refer to Hill and Hutchinson (1975) and Hutchinson and Neale (1977) for quasi-static conditions. Under dynamic conditions, Fressengeas and Molinari (1985, 1994), Shenoy and Freund (1999) developed a multidimensional linear stability analysis (modal analysis). Inertia is shown to damp long wavelengths while viscosity and multiaxiality of the flow tend to extinguish short wavelengths. At each step of the deformation process, an intermediate wavelength having the largest growth rate thus emerges and was supposed to characterize the mean neck spacing observed in experiments.

Mercier and Molinari (2003) and Mercier and Molinari (2004) respectively applied linear stability analyses to the case of cylindrical bars and tubes. Using this method, Jouve (2010) retrieved the average fragment size of the experimental work of Olive et al. (1979) on the dynamic expansion of steel cylinder. Mercier et al. (2010) analyzed the expansion of a hemispherical shell using a plate theory. In addition, Jouve (2015) studied instabilities in metallic plates under dynamic biaxial loading. A 1D formalism was also proposed in the literature where the stress multiaxiality in the neck region is accounted for by adopting the Bridgman correction factor, see for instance Zhou et al. (2006) for the dynamic stretching of round bar. Note that the neck development in biaxial loading was also investigated in Zaera et al. (2015) by considering linear stability analysis using the Bridgman correction factor Bridgman (1952). However, most of the methods are based on a frozen coefficient theory that implicitly supposes that the time evolution of the perturbation is much faster than the one of the homogeneous solution. This strong assumption is not verified for very high strain rates. Xavier et al. (2020) developed a linear stability formalism without adopting the frozen coefficient theory. Within a 2D theoretical framework, they observed that while growth rates obtained with the frozen coefficient theory are retrieved with the new development in the late stage of the deformation process, they are highly different in the early stage. This induces strong discrepancies in terms of perturbation amplitudes. Recently, Jacques (2020) proposed a two-zone model for the dynamic biaxial stretching

of a plate adopting also the Bridgman correction factor. Dynamic forming limit curves obtained with this analytical approach compared well with finite element calculations. It is also interesting to mention the approaches developed by Audoly and Hutchinson (2016) and Audoly and Hutchinson (2019) who proposed a new 1D methodology to analyze the necking of round bars and sheets in quasi-static conditions. Interestingly, they were able to find a new analytical expression of the Bridgman correction factor. As in all works of the literature, the neck retardation is influenced by positive strain hardening, strain-rate dependence and also by non-uniform stress distribution in the neck.

The aim of the paper is to revisit the development proposed in Xavier et al. (2020) by considering a 1D approach with introduction of a Bridgman correction factor. In this paper, the necking process is studied during the stretching of a rectangular plate. It will be seen in Appendix B that the theory is easily extended to describe the dynamic extension of a cylindrical rod, which is assumed in the literature to be representative of the ring expansion. In Section 2, the 1D theoretical framework based on the formalism of Zhou et al. (2006) is derived. The system of equations governing the evolution of perturbations is established. The frozen coefficient theory is not used and the time evolution of the perturbation amplitudes is governed by two differential equations: one equation for the perturbed accumulated plastic strain and one for the thermal perturbation. In Section 3, the multiple necking of a plate made of copper is analyzed. The material is exhibiting strain hardening, strain rate sensitivity and thermal softening. The difference between the proposed development and the 1D classical linear stability analysis based on the frozen coefficient theory (1D-CLSA) is revealed. The influence of the modeling of multiaxiality of the plastic flow is analyzed by comparing results obtained with the present model, referred to as 1D-XLSA and the 2D-XLSA model of Xavier et al. (2020). The role of the initial material state is also discussed.

2 Modeling

Consider a plate of initial half-length L_0, initial thickness h_0 and infinite width, see Fig.1. The initial thickness can be non uniform so that one has the possibility to explore the situation where h_0 varies along the longitudinal axis: $h_0(X)$. The plate is submitted to plane strain conditions by imposing a constant velocity V_0 to the surfaces $X = \pm L_0$:

$$v_x(\pm L_0, t) = \pm \dot{\varepsilon}_0 L_0 \quad \text{where} \quad \dot{\varepsilon}_0 = \frac{V_0}{L_0} \tag{1}$$

where $\dot{\varepsilon}_0$ represents the nominal strain rate. In the following, we assume that at any material point in the plate, the initial velocity field is : $v_x(X, t = 0) = \dot{\varepsilon}_0 X$. In this paper, a 1D approach will be presented, so the index x referring to the component or the direction will be omitted next.

The material is assumed thermo-viscoplastic. During plastic straining, the flow stress σ_Y is described as the sum of two terms: a rate insensitive thermoplastic yield stress $\sigma_Y^p(\varepsilon_p, T)$ and a viscous overstress $\sigma_Y^v(\varepsilon_p, \dot{\varepsilon}_p, T)$:

$$\sigma_Y = \sigma_Y^p + \sigma_Y^v = f(\varepsilon_p, \dot{\varepsilon}_p, T)\,, \tag{2}$$

where T is the absolute temperature. $\dot{\varepsilon}_p$ is the equivalent plastic strain rate. Since elasticity is neglected in the present approach, one has, within the von Mises theory framework, $\dot{\varepsilon}_p = \left(\frac{2}{3}\mathbf{D} : \mathbf{D}\right)^{\frac{1}{2}}$, with $\mathbf{D}$ being the strain rate tensor and (:) being the double contraction for second order tensors. $\varepsilon_p = \int_0^t \dot{\varepsilon}_p d\tau + \varepsilon_p^0$ is the accumulated plastic strain with ε_p^0 being a pre-strain parameter.

We propose to develop a 1D Lagrangian approach for the prediction of multiple necking. As a consequence, any mechanical or thermal field G, solution of the problem, is only related to the Lagrangian coordinate X and

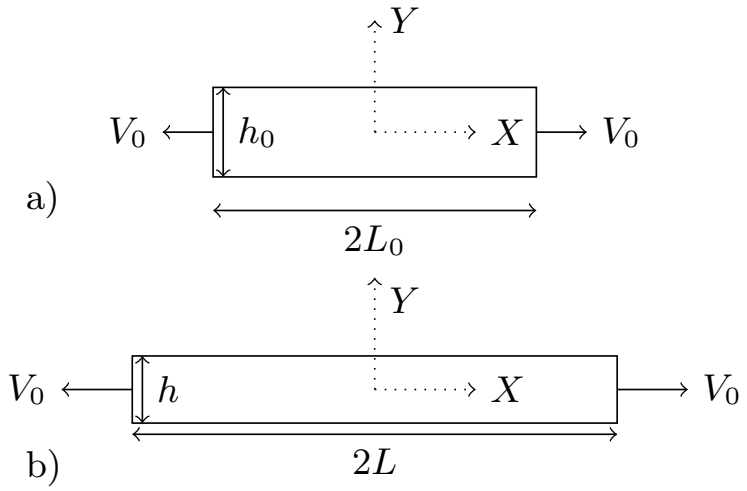

Figure 1: Schematic representation of the plate, of initial half-length L_0 and uniform initial thickness h_0 at a) initial time $t = 0$ and b) current time t. Velocities $\pm V_0$ are applied to the extremities $X = \pm L_0$. In the figure, the situation of a configuration without geometrical defects is presented.

time $t : G(X, t)$. In the following, dependencies relatively to X and t will be omitted for the sake of conciseness. The field equations are recalled below. More details can be found in Fressengeas and Molinari (1985), Zhou et al. (2006) or Rodríguez-Martínez et al. (2013a).

The conservation of linear momentum in the longitudinal direction is written as:

$$\rho_0 h_0 \frac{\partial v}{\partial t} = \frac{\partial (h\sigma)}{\partial X} \tag{3}$$

where ρ_0 is the initial mass density of the material. Incompressibility is supposed *i.e* ρ_0 is constant, and assumed uniform. v is the current velocity in the longitudinal direction, h_0 (resp. h) the initial (resp. current) plate thickness and σ the current longitudinal Cauchy stress (at time t).

From the definition of the true strain ε:

$$\varepsilon = \ln\left(\frac{\partial x}{\partial X}\right), \tag{4}$$

the continuity equation leads to:

$$\frac{\partial v}{\partial X} = \dot{\varepsilon} e^{\varepsilon} \tag{5}$$

where $\dot{\varepsilon}$ is the longitudinal strain rate and x the current position. During plane strain stretching, the thickness of the plate decreases. Elasticity being neglected and owing to volume preserving of the plastic deformation, one gets:

$$h = h_0 e^{-\varepsilon} \tag{6}$$

Under plane strain stretching, and since the material is assumed rigid plastic, the equivalent plastic strain rate $\dot{\varepsilon}_p$ is related to the longitudinal strain rate $\dot{\varepsilon}$ through:

$$\dot{\varepsilon}_p = \frac{2}{\sqrt{3}} \dot{\varepsilon} \tag{7}$$

By time integration of Eq.(7), we have:

$$\varepsilon_p - \varepsilon_p^0 = \frac{2}{\sqrt{3}}\varepsilon \tag{8}$$

To account for the multidimensional aspect of the stress field within the neck region, the 1D approach is complemented by considering the Bridgman correction for plane strain, see Bridgman (1952). Therefore the true stress σ is replaced by an average axial stress accross the plate thickness defined as:

$$\sigma = \frac{2\sigma_Y}{\sqrt{3}} B(\Phi) \tag{9}$$

where $B(\Phi)$ is the Bridgman correction factor. More details on this correction factor are presented in Appendix C. Φ is a parameter depending on the thickness profile and given by:

$$\Phi = \frac{h}{8}\frac{\partial^2 h}{\partial x^2} \tag{10}$$

When the faces ($Y = \pm h_0/2$) of the plate remain planar (homogeneous deformation of the plate with initial uniform thickness as displayed in Fig. 1), $\Phi = 0$ and $B(\Phi) = 1$. In that case, the true stress is simply $\sigma = \frac{2\sigma_Y}{\sqrt{3}}$. For limited amplitude of necks, the term $B(\Phi)$ can be approximated by its first order Taylor expansion:

$$B(\Phi) = 1 + \frac{2\Phi}{3} + o(\Phi^2) \tag{11}$$

The plate is subjected to high strain rate loading such that adiabatic conditions prevail with no heat conduction inside. Thus, heat equation reduces to:

$$\rho_0 C\dot{T} = \beta^{TQ}\sigma_Y\dot{\varepsilon}_p \tag{12}$$

where β^{TQ}, the Taylor-Quinney coefficient, represents the proportion of plastic work converted into heat. In the present work, β^{TQ} is assumed constant. Nevertheless, the present approach can be extended without difficulties to account for the evolution of β^{TQ} during the deformation process, as it has been discussed in the literature, see Mason et al. (1994), Rittel (1999), Longère and Dragon (2008) or Stainier and Ortiz (2010). C is the heat capacity of the material assumed constant in this work. Note that heat conduction might have effects for short wavelength perturbations. The characteristic time for conduction τ^{cond} related to the Fourier dimensionless number, is linked to the characteristic size of the domain and the diffusivity α. In our approach, we can assume that the shortest wavelength for necks is of the order of the plate thickness. So, one gets $\tau^{cond} \approx h_0^2/\alpha$. For a plate thickness of 1 mm and for a material representative of copper, $\tau^{cond} \approx 0.008\ s$. The assumption of adiabatic condition during multiple necking process seems to be valid for a nominal strain rate over $1000\ s^{-1}$, condition fulfilled in the present paper.

When the plate has initially a uniform thickness ($h_0(X) = h_0^b$), a homogeneous solution as presented in Fig.1 may exist. The corresponding background solution G^b, satisfying Eqs (3)-(12) with boundary conditions Eq.(1), can be expressed as follows:

$$\begin{aligned} x^b &= (1+\dot{\varepsilon}_0 t)X \quad & \varepsilon^b &= \ln(1+\dot{\varepsilon}_0 t) > 0 \\ h^b &= \frac{h_0^b}{1+\dot{\varepsilon}_0 t} & \dot{\varepsilon}_p^b &= \frac{2}{\sqrt{3}}\frac{\dot{\varepsilon}_0}{1+\dot{\varepsilon}_0 t} \\ \Phi^b &= 0 & \sigma^b &= \frac{2\sigma_Y^b}{\sqrt{3}} \end{aligned} \tag{13}$$

In the present work, at time $t = 0$, the plate thickness is non uniform. An initial thickness profile is prescribed

$h(X,t=0)=h_0(X)$. We assume that the initial thickness is the sum of the homogeneous background thickness and a small perturbation: $h_0(X) = h_0^b + \delta h_0(X)$, such that $h_0^b =< h_0(X) >$ represents the mean value of the initial thickness over the whole length of the specimen. In that case, the average value of the perturbation is vanishing $< \delta h_0(X) >= 0$. Similarly, an initial pre-strain profile $\varepsilon_p^0(X) = \varepsilon_p^{0\,b} + \delta\varepsilon_p^0(X)$ is also prescribed. This field is somehow induced by the thermo-mechanical treatment, related to the processing route or the presence of microstructural defects. Note also that as the initial longitudinal velocity field is $v(X,t=0) = \dot{\varepsilon_0}X$, the initial longitudinal strain rate $\dot{\varepsilon}^0(X)$ is uniform, equal to $\dot{\varepsilon_0}$. Necessarily, the initial perturbations in longitudinal strain rate and equivalent plastic strain rate are vanishing: $\delta\dot{\varepsilon}(X,t=0) = \delta\dot{\varepsilon}_p(X,t=0) = 0$. Finally, an initial temperature profile is prescribed: $T_0(X) = T_0^b + \delta T_0(X)$. Therefore, due to these initial pre-defined inhomogeneities in the plate, all other fields of the problem will be also initially heterogeneous. At $t=0$, the plate has not been stretched yet, meaning that the longitudinal strain is $\varepsilon(X,t=0)=0$. Therefore, $\varepsilon^b(X,t=0)=0$ and $\delta\varepsilon(X,t=0)=0$.

During the deformation process, any field G will be the sum of the homogeneous solution G^b and a time evolving perturbation $\delta G(X,t)$:

$$\begin{array}{lll} v = v^b + \delta v & \varepsilon = \varepsilon^b + \delta\varepsilon & \varepsilon_p = \varepsilon_p^b + \delta\varepsilon_p \\ h = h^b + \delta h & \sigma = \sigma^b + \delta\sigma & \sigma_Y = \sigma_Y^b + \delta\sigma_Y \\ \dot{\varepsilon} = \dot{\varepsilon}^b + \delta\dot{\varepsilon} & \Phi = \Phi^b + \delta\Phi & T = T^b + \delta T \\ \dot{\varepsilon}_p = \dot{\varepsilon}_p^b + \delta\dot{\varepsilon}_p & & \end{array} \tag{14}$$

Substituting relations (14) into the governing equations (3)-(12) and adopting the homogeneous solution defined in Eq.(13) provide a set of equations for the perturbed fields:

$$\begin{array}{ll} \dfrac{\partial\delta v}{\partial X} = e^{\varepsilon^b}\left(\dot{\varepsilon}^b\delta\varepsilon + \delta\dot{\varepsilon}\right) & \delta h = -h_0^b e^{-\varepsilon^b}\delta\varepsilon + \delta h_0 e^{-\varepsilon^b} \\ \delta\sigma = \dfrac{2\delta\sigma_Y}{\sqrt{3}} + \dfrac{4}{3\sqrt{3}}\sigma_Y^b\delta\Phi & \rho_0 h_0^b\dfrac{\partial\delta v}{\partial t} = h^b\dfrac{\partial\delta\sigma}{\partial X} + \sigma^b\dfrac{\partial\delta h}{\partial X} \\ \delta\Phi = \dfrac{h^b\exp(-2\varepsilon^b)}{8}\dfrac{\partial^2\delta h}{\partial X^2} & \delta\dot{\varepsilon}_p = \dfrac{2}{\sqrt{3}}\delta\dot{\varepsilon} \\ \delta\varepsilon_p = \dfrac{2}{\sqrt{3}}\delta\varepsilon + \delta\varepsilon_p^0 & \delta\sigma_Y = \sigma_{Y,\varepsilon_p}^b\delta\varepsilon_p + \sigma_{Y,\dot{\varepsilon}_p}^b\delta\dot{\varepsilon}_p + \sigma_{Y,T}^b\delta T \\ \rho_0 C\delta\dot{T} = \beta^{TQ}(\dot{\varepsilon}_p^b\delta\sigma_Y + \sigma_Y^b\delta\dot{\varepsilon}_p) & \end{array} \tag{15}$$

where $\sigma_{Y,\omega}^b$ denotes the partial derivative of σ_Y^b with respect to the variable ω (ω being ε_p, $\dot{\varepsilon}_p$ or T).

A modal analysis is carried out. As in Xavier et al. (2020), any perturbation field δG is searched of the form $\delta G(X,t) = \cos(\gamma X)\hat{G}(\gamma,t)$, (except for the perturbation of the velocity whose form is $\delta v = \sin(\gamma X)\hat{v}(\gamma,t)$, see Eq.3) where γ is the longitudinal wavenumber of the perturbation. The prescribed mathematical description of perturbation fields is to the author's point of view compatible with the studied configuration where a material defect is imposed. Indeed, the plate has a non uniform thickness $h_0(X)$, of sinusoidal shape with longitudinal wavenumber γ. In the literature, some recent contributions (see Ravi-Chandar and Triantafyllidis (2015) or Vaz-Romero et al. (2017)) have analyzed the dynamic stretching of a homogeneous configuration where a localized defect in velocity and strain rate was introduced. In that specific case, the propagation of the defect in the sample

prior to a phase where well defined necks occur was observed. By adopting the above form $\delta G(X,t)$, we are not able to analyze the propagation of such localized defect. This is not our goal. It has been checked by finite element calculations, that the stretching of a plate with a non uniform thickness (pattern with a single wavenumber γ) does not lead to propagation phenomena of the material defect.

To satisfy the boundary condition Eq.(1) (*i.e.* $\delta v(X=\pm L_0,t)=0$), the wavenumber γ is related to the initial length of the plate by: $\gamma L_0 = k\pi$ (k is an integer representing the initial number of necks along the X direction). Functions $\hat{G}$ depend only on time and wavenumber γ, and may have positive or negative value. Their absolute values represent the true amplitude of each perturbation field. Nevertheless, in the following $\hat{G}$ will be named amplitudes. From now on, their dependencies on γ will be omitted for the sake of conciseness. In our analysis, the time dependency of $\hat{G}$ is not enforced to be of exponential form (as in Zhou et al. (2006) or Rodríguez-Martínez et al. (2013a)). In that sense, the proposed methodology is similar to the one recently proposed by Xavier et al. (2020). Nevertheless, contrary to Xavier et al. (2020) in which a 2D approach is derived, the present work is restricted to the development of a 1D approach.

The ten perturbed quantities (δv, $\delta\varepsilon$, $\delta\dot{\varepsilon}$, $\delta\varepsilon_p$, $\delta\dot{\varepsilon}_p$, δh, $\delta\sigma$, $\delta\sigma_Y$, $\delta\Phi$ and δT) or equivalently the associated amplitudes ($\hat{v}$, $\hat{\varepsilon}$, $\dot{\hat{\varepsilon}}$, $\hat{\varepsilon}_p$, $\dot{\hat{\varepsilon}}_p$, $\hat{h}$, $\hat{\sigma}$, $\hat{\sigma}_Y$, $\hat{\Phi}$ and $\hat{T}$) are related to each other owing to the nine relationships of Eqs (15). In this set of equations, the terms $\delta\varepsilon_p^0$ and δh_0 (and the associated amplitudes $\hat{\varepsilon}_p^0$ and $\hat{h}_0$) are initial prescribed quantities.

Next, as in Xavier et al. (2020), a mechanical perturbation (here represented by the perturbation in accumulated plastic strain $\hat{\varepsilon}_p$) and a thermal perturbation (here $\hat{T}$) are selected to be representative of the perturbation. Note that another choice could have been possible for the mechanical perturbation but the present choice is the one that leads to the simplest derivation. After adequate combinations, the set of Eqs (15) reduces to only two ordinary differential equations coupling the perturbation amplitude $\hat{\varepsilon}_p$ of the accumulated plastic strain and the perturbation amplitude $\hat{T}$ of the temperature:

$$a_1\ddot{\hat{\varepsilon}}_p + a_2\dot{\hat{\varepsilon}}_p + a_3\hat{\varepsilon}_p + a_4\hat{T} = s_0 \qquad \dot{\hat{T}} = b_1\hat{T} + b_2\dot{\hat{\varepsilon}}_p + b_3\hat{\varepsilon}_p \tag{16}$$

Coefficients a_i and b_i in Eq.(16) are only time dependent, related to the homogeneous solution:

$$\begin{aligned}
a_1(t) &= \rho_0\frac{1+\dot{\varepsilon}_0 t}{2}\sqrt{3} & b_1(t) &= \beta^{TQ}\frac{2\dot{\varepsilon}_0}{\rho_0 C\sqrt{3}(1+\dot{\varepsilon}_0 t)}\sigma^b_{Y,T}\\
a_2(t) &= \rho_0\sqrt{3}\dot{\varepsilon}_0 + \frac{2\gamma^2}{\sqrt{3}(1+\dot{\varepsilon}_0 t)}\sigma^b_{Y,\dot{\varepsilon}_p} & b_2(t) &= \frac{\beta^{TQ}}{\rho_0 C}\left(\frac{2\dot{\varepsilon}_0}{\sqrt{3}(1+\dot{\varepsilon}_0 t)}\sigma^b_{Y,\dot{\varepsilon}_p} + \sigma^b_Y\right)\\
a_3(t) &= \frac{2\gamma^2}{\sqrt{3}(1+\dot{\varepsilon}_0 t)}\sigma^b_{Y,\varepsilon_p} + \frac{\left(h_0^b\right)^2\sigma^b_Y}{12(1+\dot{\varepsilon}_0 t)^5}\gamma^4 - \frac{\gamma^2\sigma^b_Y}{1+\dot{\varepsilon}_0 t} & b_3(t) &= \beta^{TQ}\frac{2\dot{\varepsilon}_0}{\rho_0 C\sqrt{3}(1+\dot{\varepsilon}_0 t)}\sigma^b_{Y,\varepsilon_p}\\
a_4(t) &= \frac{2\gamma^2}{\sqrt{3}(1+\dot{\varepsilon}_0 t)}\sigma^b_{Y,T}
\end{aligned} \tag{17}$$

s_0 is a time dependent coefficient that depends also on the prescribed amplitudes $\hat{h}_0$ and $\hat{\varepsilon}_p^0$:

$$s_0 = \left(\frac{\hat{h}_0}{h_0^b} + \frac{\sqrt{3}}{2}\hat{\varepsilon}_p^0\right)\left[\frac{\left(h_0^b\right)^2\gamma^4\sigma^b_Y}{6\sqrt{3}(1+\dot{\varepsilon}_0 t)^5} - \frac{2\sigma^b_Y\gamma^2}{\sqrt{3}(1+\dot{\varepsilon}_0 t)}\right] \tag{18}$$

The system (16) is composed respectively of a second order and of a first order ordinary differential equations for $\hat{\varepsilon}_p$ and $\hat{T}$. Thus, initial conditions $\hat{\varepsilon}_p(t=0)$, $\dot{\hat{\varepsilon}}_p(t=0)$ and $\hat{T}(t=0)$ are required. However, as stated previously, due to the initial conditions on the imposed strain rate field, necessarily, $\dot{\hat{\varepsilon}}_p(t=0)=0$.

The system (16) is solved using a finite difference scheme with a splitting strategy in which each differential equation is solved successively within a timestep. A convergence study revealed that predictions are converged for sufficiently small timesteps. Remember that one of the main interest of the proposed work is that time evolutions of perturbation amplitudes are direct outcomes of the model.

As already mentioned, in the linear stability analysis of the literature with Bridgman correction factor as in Zhou et al. (2006) or in Rodríguez-Martínez et al. (2013a) (in the case of a cylindrical bar) or Zaera et al. (2015) (in the case of biaxial stretching of a plate), a frozen coefficient theory is used and $\hat{G}(t)$ is assumed of exponential form: $\hat{G}(t) = \hat{G}_o e^{\eta t}$ with η being the instantaneous growth rate of the perturbation and $\hat{G}_o$ the initial amplitude. In that case, all fields have the same growth rate. The governing equation for the instantaneous growth rate η is developed in Appendix A. By performing the linear stability analysis at various consecutive times, the amplitude of any perturbation field $\hat{G}$ is estimated by the relation $\hat{G} = \hat{G}^0 \exp(\int_{t_1}^{t} \eta d\tau)$, where t_1 is the first time during the deformation process where the growth rate η becomes positive, see Petit et al. (2005), El Maï (2014) or Vaz-Romero et al. (2017). Implicitly, we assume in this paper that before t_1, the perturbation is not evolving. Of course, this is a crude assumption and it could be of interest to investigate the response of the classical linear stability analysis in a configuration where non positive growth rate is captured. This is not the subject of the present paper and this work is currently under investigation. With this type of approach, the relative amplitudes (defined as the ratio between the current and the initial amplitudes) of all fields are identical.

With the proposed extended Bridgman analysis, the amplitudes $\hat{\varepsilon}_p$ and $\hat{T}$ are natural outcomes of the model. As seen in Xavier et al. (2020), there is no simple link between them except their combined interaction inherited from the thermo-mechanical coupling and described by Eqs (16). As a consequence, their respective growth rates are not identical. We define the instantaneous growth rate of the mechanical perturbation $\eta_{\hat{\varepsilon}_p}$ by:

$$\eta_{\hat{\varepsilon}_p}(\gamma, t) = \frac{\dot{\hat{\varepsilon}}_p}{\hat{\varepsilon}_p} \tag{19}$$

which is depending on time t and the wavenumber γ. In the following, the dependency upon t and γ will be omitted for the sake of conciseness. As in Xavier et al. (2020), the instantaneous growth rate of the thermal perturbation $\eta_{\hat{T}}(\gamma, t) = \frac{\dot{\hat{T}}}{\hat{T}}$ could have been also introduced. Nevertheless, a comparison between the mechanical and thermal growth rate leads to trends similar to those observed in Xavier et al. (2020). So, results concerning the thermal growth rate evolution are not shown in the present work.

3 Results

In the present work, the initial thickness is not uniform. The thickness perturbation will be of sinusoidal shape: $\delta h_0(X) = \cos(\gamma X)\hat{h}_0$. $\hat{h_0}$ is the amplitude of the thickness perturbation.The plate has the following dimensions: $L_0 = 180.8\ mm$, $h_0^b = 2.4\ mm$ and $\hat{h}_0 = 8\ \mu m$. The initial longitudinal strain rate $\dot{\varepsilon}_0$ is $= 2300\ s^{-1}$, *.i.e.* $\dot{\varepsilon}_X(X, t = 0) = \dot{\varepsilon}_0$.

The material, representative of copper, has a thermo-viscoplastic behavior modeled by a power law, see Mercier et al. (2010):

$$\sigma_Y = K\varepsilon_p^n \dot{\varepsilon}_p{}^m T^{-q} \tag{20}$$

Values for the hardening coefficient n, the strain rate sensitivity parameter m and the thermal softening parameter q are taken from Mercier et al. (2010) and given in Table (1). For the calculations, the value $\beta^{TQ} = 1$ is

selected.

$\rho_0(\ kg/m^3)$	$C(J/kg/K)$	$K(I.S.)$	n	m	q	β^{TQ}	$T_0(K)$	${\varepsilon_p^0}^b$
8930	383	$1.075\ 10^9$	0.35	0.0098	0.111	1	300	0.256

Table 1: Material parameters for copper taken from Mercier et al. (2010). The flow stress is described by a powerlaw, see Eq.(20)*.*

As mentioned in the previous section, initial conditions for the temperature and pre-strain are compulsory. Owing to the initial longitudinal velocity field Eq. (1), the perturbation in strain rate has initially a zero amplitude: $\dot{\hat{\varepsilon}}_p(t=0)=0$. In the following of the paper, the initial temperature field and pre-strain are non uniform: $T_0(X) = T_0^b + \delta T_0(X)$ and $\varepsilon_p^0(X) = {\varepsilon_p^0}^b + \delta\varepsilon_p^0(X)$. As for the plate thickness, initial perturbations in temperature and accumulated plastic strain (named also pre-strain at $t=0$) are of sinusoidal shape: $\delta T_0(X) = \cos(\gamma X)\hat{T}_0$ and $\delta\varepsilon_p^0(X) = \cos(\gamma X)\hat{\varepsilon}_p^0$. Throughout the paper, we will consider for illustrative purpose that $\hat{T}(t=0) = \hat{T}_0 = 4\ K$ and $\hat{\varepsilon}_p(t=0) = \hat{\varepsilon}_p^0$ (to be defined). In addition, as in Xavier et al. (2020), we enforce a link between the initial perturbed quantities for the thickness and the plastic strain such that,

$$\delta\varepsilon_p^0(X) = -\frac{2}{\sqrt{3}}\frac{\delta h_0(X)}{h_0^b} \tag{21}$$

From Eq.(21) and the prescribed value of $\hat{h}_0 = 8\ \mu m$, we found: $\hat{\varepsilon}_p^0 = -3.85.10^{-3}$. In fact, by considering the above relationship, one observes from Eq.(18) that $s_0 = 0$. As a consequence, the set of differential equations (16) is slightly simplified. Nevertheless, the complete theory has been derived without such a link and no relationship is necessary between $\hat{h}_0$ and $\hat{\varepsilon}_p^0$. In addition, the adopted initial conditions are consistent with the ones used in Xavier et al. (2020) where a similar relation between the perturbation of the plate thickness and the perturbation of the pre-strain was considered.

To provide an evaluation of the traction force needed to stretch the plate dynamically, we propose to display its evolution for the background solution (determined with the condition of uniform thickness h_0^b). In that case, from Eq. (13), the plastic strain within the plate is : $\varepsilon_p^b = {\varepsilon_p^0}^b + \frac{2}{\sqrt{3}}\ln(1+\dot{\varepsilon}_0 t)$. The temperature evolution is governed by Eq. (12). As a consequence, the force F^b applied at the lateral surfaces $X = \pm L_0$ (per unit width) is defined as:

$$F^b = \sigma^b h^b = \frac{2}{\sqrt{3}}\sigma_Y^b h_0^b e^{-\varepsilon^b} \tag{22}$$

Of course, when a perturbation is introducted, the force will be changed, mostly after the maximum of the force is reached.

Fig.2 displays the time evolution of the normalized force F^b/F_{max} for a plate of uniform thickness under nominal strain rate $\dot{\varepsilon}_0 = 2300\ s^{-1}$. For the parameters adopted in the present paper (see Table 1), the force first increases and reaches its maximum value at around $t = 50\ \mu s$. It will be checked that for non homogeneous plates as considered next, the amplification of the perturbation is mainly observed for time larger than $50\ \mu s$.

3.1 Growth rate and amplitude estimations

In this section, the predictions of the evolution of the perturbation are derived with our new model. In that case, the time evolution of the perturbation amplitude does not have a predefined exponential form as in the 1D-CLSA theory, and is evolving according to a system of ordinary differential equations. We propose thus to compare results

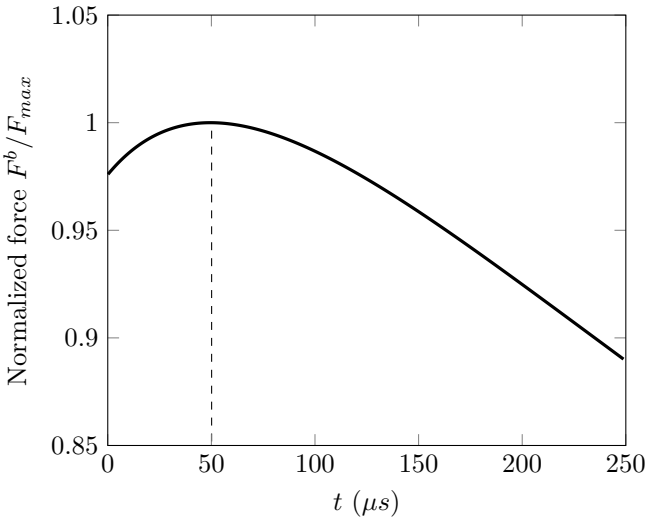

Figure 2: Time evolution of the normalized force F^b/F_{max} registered at $X = \pm L_0$ by unit width, see Eq.(22)*. Plane strain conditions are prescribed. Thermo-mechanical coupling is accounted for. The material is thermoviscoplastic, with a powerlaw flow stress, see Eq.*(20)*. Material parameters are listed in Table 1. The nominal strain rate is* $2300\ s^{-1}$*. The plate is homogeneous with uniform thickness.*

obtained from the 1D-XLSA and 1D-CLSA approaches.

Fig. 3 represents a) the normalized growth rate $\eta_{\hat{\varepsilon}_p}/\dot{\varepsilon}_0$ and b) the normalized amplitude $|\frac{\hat{\varepsilon}_p}{\hat{\varepsilon}_p^o}|$ as a function of the normalized wavenumber γh_0^b at $t = 200\ \mu s$. As mentioned in Fressengeas and Molinari (1994), Shenoy and Freund (1999) or Mercier and Molinari (2003), an intermediate wavenumber γ_a for which the growth rate is maximum is selected due to the combined effect of inertia, viscosity and stress triaxiality, see Fig.3a). A second dominant wavenumber γ_b is observed for the amplitude in Fig.3b). The two dominant modes (defined via a criterion based on the critical growth rate or amplitude) are different: $\gamma_a = 2.2/h_0^b$ and $\gamma_b = 1.54/h_0^b$. This result, already observed in El Maï (2014), may have some influence on the estimated number of necks since in the literature, either a criterion based on a critical normalized growth rate (for instance in Shenoy and Freund (1999)) or on a critical normalized amplitude (for instance in El Maï et al. (2014) or Vaz-Romero et al. (2017)) can be found. In Vaz-Romero et al. (2017), the case of a non-linear elastic rod under dynamic stretching was analyzed by finite element calculations and by using the 1D-CLSA model. The authors have shown that the criterion based on the amplitude was relevant to reproduce the neck spacing observed in calculations. Further works are necessary to confirm this result.

Fig.3a) also shows that growth rates obtained at $t = 200\ \mu s$ adopting the proposed approach derived from Eq.(16) or the linear stability analysis based on the frozen coefficient assumption (1D-CLSA, see Appendix A) are similar at least for wavenumbers $0.3/h_0^b \leq \gamma \leq 2.4/h_0^b$. For perturbation modes with wavenumber close to $\gamma_I = 0.13/h_0^b$, growth rates predicted by the 1D-XLSA model are large as displayed in Fig.3a) with the dashed vertical asymptotic line. As discussed in Xavier et al. (2020), the large value of the growth rate defined in Eq.(19) is due to the fact that the amplitude of the perturbation vanishes for γ_I, see Fig.3b). Fig.3b) shows that amplitudes are clearly different from one model to another, while both models lead to the same dominant wavenumber, *i.e* $\gamma_b = 1.54/h_0^b$. Indeed, with the proposed approach, the normalized amplitude for the dominant mode is close to 270 while with the 1D-CLSA, the normalized amplitude is around 58, more than four times smaller. Remember that at time $t = 200\ \mu s$, growth rates predicted by the two approaches are identical for the dominant mode γ_a, see

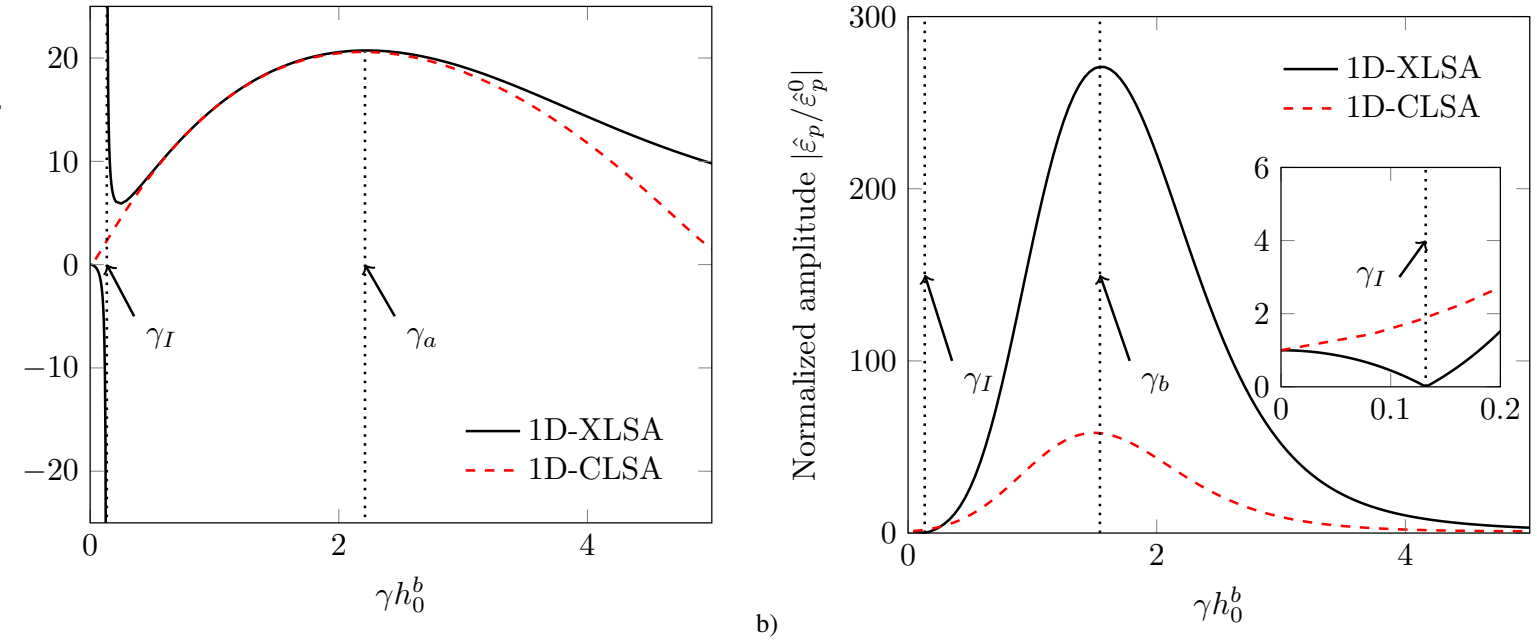

Figure 3: a) Normalized growth rate $\eta_{\hat{\varepsilon}_p}/\dot{\varepsilon}_0$ and b) normalized amplitude $|\frac{\hat{\varepsilon}_p}{\hat{\varepsilon}_p^o}|$ as a function of the normalized wavenumber γh_0^b at $t = 200\ \mu s$. The zoomed part for small wavenumbers in b) illustrates the fact that amplitude tends to zero for the wavenumber γ_I. The material is thermoviscoplastic, with a powerlaw flow stress, see Eq.(20). Material parameters are listed in Table 1. The nominal strain rate is $\dot{\varepsilon}_0 = 2300\ s^{-1}$. Initial thickness is $h_0^b = 2.4\ mm$. Initial amplitude of the thickness perturbation is $\hat{h}_0 = 8\ \mu m$.

Fig. 3a). This amplitude difference is solely due to history effect, so large differences in growth rate may exist at the early stage of the deformation process. This result in terms of amplitude was already stated in Xavier et al. (2020) when comparing 2D linear stability approaches.

Fig.4 presents the time evolution of a) the normalized growth rate $\eta_{\hat{\varepsilon}_p}/\dot{\varepsilon}_0$ and b) the normalized amplitude $|\frac{\hat{\varepsilon}_p}{\hat{\varepsilon}_p^o}|$ for $\gamma_b = 1.54/h_0^b$, shown to be the dominant wavenumber (in terms of amplitude) at $t = 200\ \mu s$. Fig.4a) shows that with the proposed 1D-XLSA model, the growth rate of the perturbation is initially negative. Therefore, the perturbation amplitude first decreases as observed on Fig.4b). At around $t_I = 12\ \mu s$, the amplitude is almost approaching zero. As the amplitude is close to zero and the growth rate $\dot{\hat{\varepsilon}}_p$ has a finite value, the corresponding normalized growth rate $\eta_{\hat{\varepsilon}_p}(t)$ defined in Eq.(19) reaches a very large value. For $t > 12\ \mu s$, $\eta_{\hat{\varepsilon}_p}(t)$ is always positive. So the amplitude of the perturbation increases. The initial amplitude is retrieved at $t = 22.5\ \mu s$. This amplitude increase occurs when the force is still increasing in Fig. 2. An important outcome from our model is therefore the capability to predict the perturbation evolution at any deformation stage. It has been checked (results not presented here) that, for all wavenumbers, the perturbation amplitude is varying during the phase of stable flow (here $t < 50\ \mu s$). For some wavenumbers, contrary to the situation presented here for $\gamma_b = 1.54/h_0^b$, the perturbation amplitude becomes larger than the initial amplitude beyond $t > 50\ \mu s$. When the 1D-CLSA model is adopted, it is seen that the normalized growth rate has limited value up to $t = 50\ \mu s$. So far, in the literature, the 1D-CLSA model has been used to investigate multiple necking mainly when the plastic flow is unstable, for which $\eta/\dot{\varepsilon}_0 >> 1$ (see Jouve (2013) for further details). As already mentioned, a specific analysis of the response of the classical linear stability analysis for stable or slightly unstable flows will be conducted in the near future. Meanwhile, in this paper, the amplitude of perturbation associated to the 1D-CLSA model will be assumed frozen, roughly up to $t = 50\ \mu s$. For $t = 100\ \mu s$, the normalized growth rate $\eta/\dot{\varepsilon}_0$ predicted based

on the 1D-CLSA approach is around 10 while with the proposed approach, the value $\eta_{\dot{\varepsilon}_p}/\dot{\varepsilon}_0$ is close to 12.8. At still $t = 100\ \mu s$, the relative amplitude for the proposed approach is 6.47 and only 1.64 with the 1D-CLSA theory. Later at $t = 200\ \mu s$, both growth rates $\eta_{\dot{\varepsilon}_p}$ and η coincide. Nevertheless, in terms of amplitude, a difference still exists; the amplitude predicted by the proposed model being 4.4 times larger than the one obtained with the 1D-CLSA model. This comparison shows clearly the importance of the early deformation stage, which may strongly influence the perturbation evolution. For predicting capability of the number of necks and most important, for the time scenario of fragmentation, this difference in amplitude may be important. Indeed, if we consider that necks start to trigger intense localization process when the normalized amplitude of the defect has reached a ratio of 30 (arbitrary value taken here only for illustrative purpose), Fig.4b) shows that this stage will be initiated at $t = 147\ \mu s$ for the present model while it is delayed up to $t = 182\ \mu s$ with the 1D-CLSA based on the frozen theory coefficient. Further work is necessary to compare predictions of the new model and finite element calculations to understand how the present model may provide new insights in the fragmentation process and predictions of neck spacing.

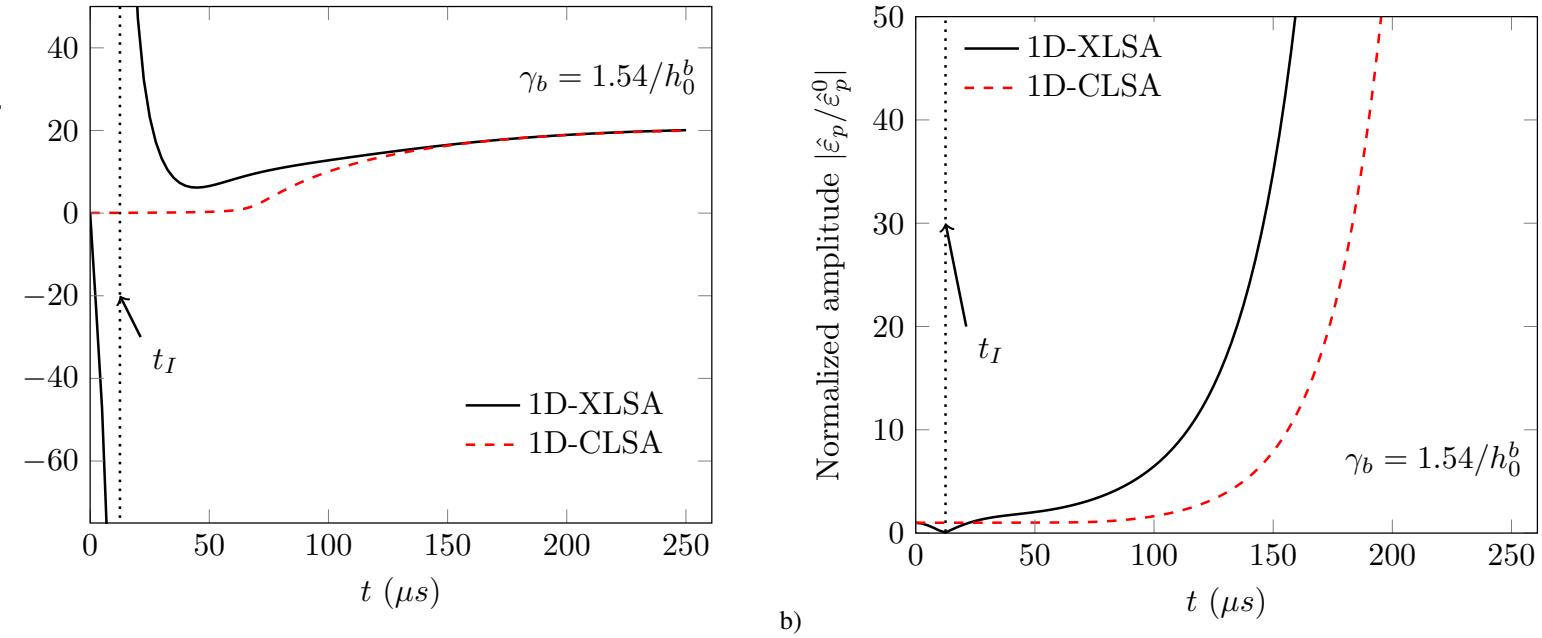

Figure 4: Time evolution of a) the normalized growth rate $\eta_{\dot{\varepsilon}_p}/\dot{\varepsilon}_0$ and b) the normalized amplitude $|\frac{\hat{\varepsilon}_p}{\hat{\varepsilon}_p^o}|$ for the 1D-XLSA model and for the 1D-CLSA model. Results are provided for the specific wavenumber γ_b. The vertical dashed line observed for time t_I is due to the observation that the predicted amplitude for the perturbation vanishes. The material is thermoviscoplastic, with a powerlaw flow stress, see Eq.(20). Material parameters are listed in Table 1. The nominal strain rate is $2300s^{-1}$. Initial thickness is $h_0^b = 2.4\ mm$. Initial amplitude of the thickness perturbation is $\hat{h}_0 = 8\ \mu m$.

3.2 Role of multiaxiality modeling and of initial plastic strain perturbations

By construction, spatial heterogeneity of initial conditions may lead to difference in perturbation evolution. We propose in the following to investigate this aspect via a comparison between predictions of the proposed 1D-XLSA model, where the through thickness dependency of fields is disregarded, and of the 2D-XLSA model where this dependency is kept. In brief (more details can be found in Xavier et al. (2020)), any perturbation fields in the 2D-XLSA model can be written as $\delta G^{2D-XLSA}(X, Y, t) = F(\gamma X)\hat{G}^{2D-XLSA}(\gamma, Y, t)$ where Y is the Lagrangian coordinate in the transversal direction. The function $F(\gamma X)$ is of sinusoidal shape and $\hat{G}^{2D-XLSA}(\gamma, Y, t)$

represents the perturbation in the transversal direction and depends on the mode γ. In the rest of the paper, the dependence of $\hat{G}^{2D-XLSA}$ on γ will be omitted for the sake of notation conciseness. Initial conditions for the perturbation not only consist in providing the initial amplitude of $\hat{G}^{2D-XLSA}$ but also in defining the spatial variation of the initial perturbation along the transversal direction. In Xavier et al. (2020), the evolution of each perturbation related to mechanical variables is associated to a stream function $\psi^{2D-XLSA}(X,Y,t)$ whose through-thickness variation is $\hat{\psi}^{2D-XLSA}(Y,t)$. The through-thickness variation of the perturbed temperature is $\hat{T}^{2D-XLSA}(Y,t)$. In particular, the through-thickness variation of the amplitude of the accumulated plastic strain perturbation is associated with the stream function as shown below:

$$\hat{\varepsilon}_p^{2D-XLSA}(Y,t) = \frac{2\gamma}{\sqrt{3}} \frac{\partial \hat{\psi}^{2D-XLSA}}{\partial Y} \tag{23}$$

For the 2D-XLSA model, initial conditions are specified by prescribing the initial shape of three quantities: $\hat{\psi}^{2D-XLSA}(Y,t=0)$, $\dot{\hat{\psi}}^{2D-XLSA}(Y,t=0)$ and $\hat{T}^{2D-XLSA}(Y,t=0)$. To be consistent with the present work, we select $\dot{\hat{\psi}}^{2D-XLSA}(Y,t=0)=0$ (no initial perturbation of the strain rate) and $\hat{T}^{2D-XLSA}(Y,t=0)=4\ K$.

In the first test, we defined initial condition $IC1$ by considering the specific form of the stream function: $\hat{\psi}^{2D-XLSA}(Y,t=0) = \dfrac{\sqrt{3}\hat{\varepsilon}_p^0}{2\gamma} Y = -\dfrac{\hat{h}_0}{2\gamma}\dfrac{2Y}{h_0^b}$. It is clear from Eq.(23) that $IC1$ case leads to an homogeneous perturbation amplitude of the accumulated plastic strain across the thickness: $\hat{\varepsilon}_p^{2D-XLSA}(Y,t=0)=\hat{\varepsilon}_p^o$, see Fig. 5. This value is the one adopted as the initial amplitude of the plastic strain perturbation in the 1D-XLSA model, see previous results. Therefore, a fair comparison between the proposed model and the 2D-XLSA approach with $IC1$ can be made. A second initial condition, $IC2$, is proposed with a pronounced fluctuation along the through thickness direction: $\hat{\psi}^{2D-XLSA}(Y,t=0) = -\dfrac{\hat{h}_0}{2\gamma}\dfrac{\sin(\omega\pi 2Y/h_0^b)}{\sin(\omega\pi)}$ with $\omega=\frac{4}{3}$ for $IC2$. As a consequence, the initial accumulated plastic strain perturbation for $IC2$ is oscillatory in the plate thickness, see Fig.5, leading to initial material heterogeneity.

Fig.6 presents the evolution of the normalized amplitude of the plastic strain perturbation as a function of the normalized wavenumber γh_0^b at $t=200\ \mu s$. First, the dominant wavenumber predicted by the 2D-XLSA model is slightly affected by the adopted initial conditions. Its value is around $\gamma \simeq 1.54/h_0^b$, and is consistent with the one obtained from the 1D-XLSA, see Fig.3b). Nevertheless, a difference in terms of amplitude exists. In that case, the difference in amplitude from the 1D-XLSA and 2D-XLSA with $IC1$ condition, is due to a difference in modeling strategy for the stress triaxiality which develops in the neck. In 1D-XLSA, the Bridgman correction factor is introduced while for the 2D-XLSA theory, the multi-dimensional aspect of the stress-field is by construction present in the model. A larger difference is observed with $IC2$. Indeed, the initial condition generates an oscillatory plastic strain in the cross-section, see Fig. 5. The material heterogeneity will induced an additional stress heterogeneity in the neck region. It could be important to evaluate how the initial material heterogeneity affects predictions for other material constitutive responses. Preliminary calculations have been carried out (results not presented here) and it has been observed that for a viscoplastic material (behavior without strain hardening and thermal softening, other material parameters being kept), no difference in growth rate prediction was observed between IC1 and IC2 for the 2D-XLSA method. Differences in predictions based on the 1D-XLSA and 2D-XLSA methods were present for large wavenumbers. For small wavenumbers, both models led to consistent results. A deeper analysis is needed and will be done in a future work.

It is also interesting to notice that for small wavenumbers, the proposed 1D-XLSA model and the 2D-XLSA approach with different initial conditions lead to the same results (at least for $\gamma h_0^b < 1$). Indeed, it is known from

the literature (see for instance Fressengeas and Molinari (1994)) that the damping of the amplitude of perturbation mode with small wavenumber is mostly due to inertia. This inertia effect is present in all models. On the contrary, for perturbations with a large wavenumber, a clear difference exists between all modeling routes considered in the work. It is also known from Fressengeas and Molinari (1994) that modes with a large wavenumber are damped mostly because of the multi-dimensionality of the flow inside the neck together with the viscoplastic properties of the material. With $IC2$ condition, the heterogeneity of the stress field in the neck is enlarged because of the initial material heterogeneity induced by the heteregeneous plastic strain field. This situation provides a clear understanding of the respective role of stress triaxiality in the neck region and also on the role of the material heterogeneity.

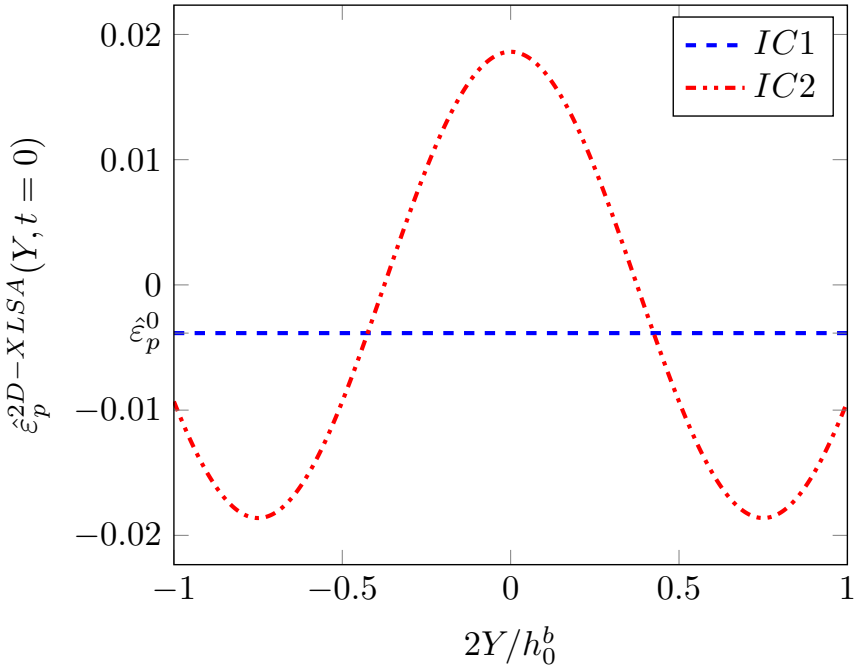

Figure 5: Spatial variation of the initial perturbation of the accumulated plastic strain along the transversal direction. The two initial conditions $IC1$ and $IC2$ are displayed. Those initial conditions for the plastic strain are induced by the stream function $\hat{\psi}^{2D-XLSA}$, see Eq.(23)*. Initial thickness is $h_0^b = 2.4\ mm$. Initial amplitude of the thickness perturbation is $\hat{h}_0 = 8\ \mu m$. Initial amplitude of the perturbation for $IC1$ is $\hat{\varepsilon}_p^0 = -0.00385$.*

Fig.7 presents the time evolution of a) the normalized amplitude $|\hat{\varepsilon}_p/\hat{\varepsilon}_p^0|$ and b) the normalized growth rate $\eta_{\hat{\varepsilon}_p}$ defined in Eq.(19) of the perturbed plastic strain for the wavenumber $\gamma_2 = 2.5/h_0^b$. The evolution of the perturbation is highly dependent on the initial conditions. Results obtained by the 1D-XLSA are close to those obtained with the 2D-XLSA model and initial condition $IC1$. In that configuration, the amplitude decreases, vanishes for $t = 8.7\ \mu s$ and then increases. Normalized amplitudes derived with initial condition $IC2$ vanishe later, at $t = 69\ \mu s$. Such a difference in the early stage of the deformation is transfered to later stage. Fig.7b) depicts the time evolution of the normalized mechanical growth rate $\frac{\eta_{\hat{\varepsilon}_p}}{\dot{\hat{\varepsilon}}_0}$ (see Eq.19) for $\gamma_2 = 2.5/h_0^b$. For the 2D-XLSA model, the mechanical growth rate is defined in Xavier et al. (2020) based on the value of the stream function and its time derivative at the upper surface of the plate: $\eta_{\hat{\varepsilon}_p}^{2D-XLSA} = \dfrac{\dot{\hat{\psi}}^{2D-XLSA}(Y = h_0/2, t)}{\hat{\psi}^{2D-XLSA}(Y = h_0/2, t)}$. Results are plotted only for the time interval where the growth of the perturbation in plastic strain remains positive. This restriction in time interval is made on purpose to avoid infinite growth rate inherited from the definition of the growth rate

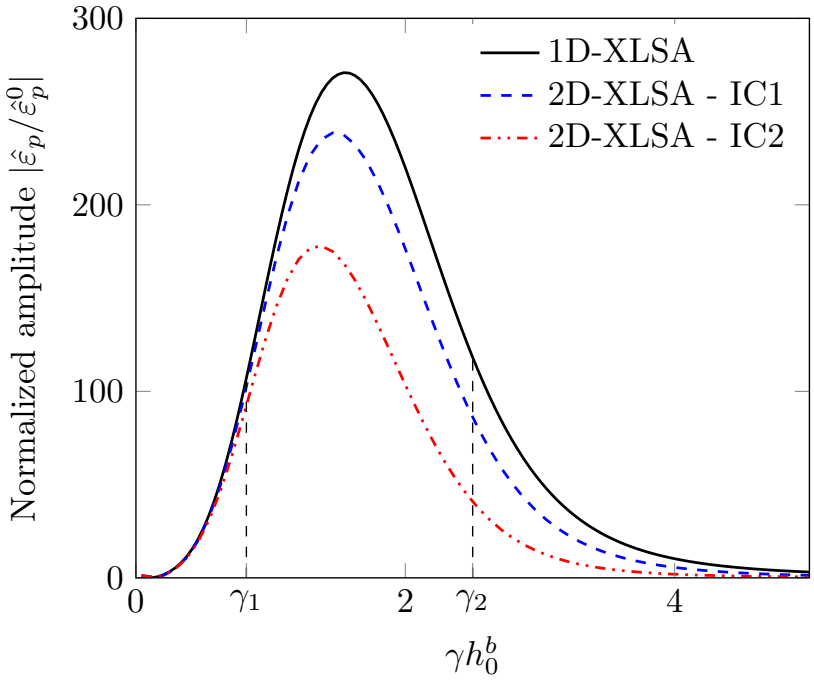

Figure 6: Normalized amplitude $|\frac{\hat{\varepsilon}_p}{\hat{\varepsilon}_p^o}|$ as a function of the normalized wavenumber γh_0^b at $t = 200\ \mu s$. A comparison between predictions of the 2D-XLSA model with various initial conditions and of the 1D-XLSA is performed. The material is thermoviscoplastic, with a powerlaw flow stress, see Eq.(20). Material parameters are listed in Table 1. The nominal strain rate is $\dot{\varepsilon}_0 = 2300\ s^{-1}$. Initial thickness is $h_0^b = 2.4\ mm$. Initial amplitude of the thickness perturbation is $\hat{h}_0 = 8\ \mu m$.

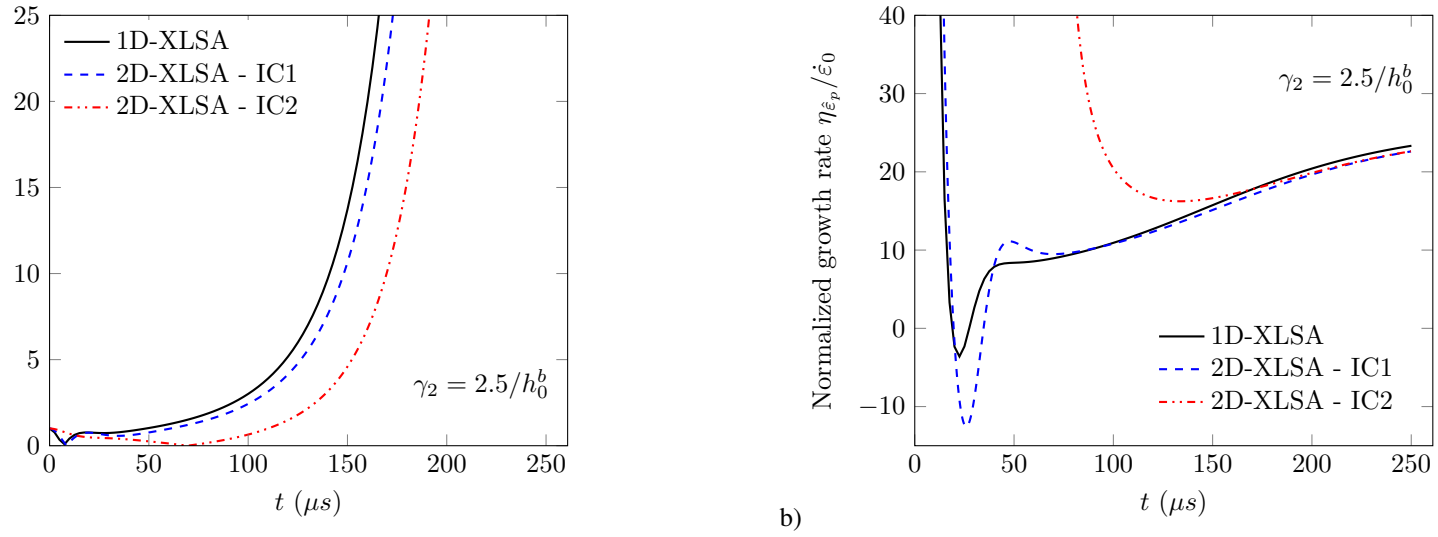

b)

Figure 7: Evolution of a) the normalized amplitude $|\hat{\varepsilon}_p/\hat{\varepsilon}_p^0|$ and b) the normalized growth rate $\eta_{\hat{\varepsilon}_p}$ defined in Eq.(19) of the perturbed plastic strain as a function of time. The wavenumber considered is $\gamma_2 = 2.5/h_0^b$. The predictions of the 2D-XLSA model with the two initial conditions are compared to the 1D-XLSA. The material is thermoviscoplastic, with a powerlaw flow stress, see Eq.(20). Material parameters are listed in Table 1. The nominal strain rate is $\dot{\varepsilon}_0 = 2300\ s^{-1}$. Initial thickness is $h_0^b = 2.4\ mm$. Initial amplitude of the thickness perturbation is $\hat{h}_0 = 8\ \mu m$.

in Eq.(19) when the amplitude is close to zero. It is seen that the time duration of the deformation process with negative growth rate is varying from $t = 8.5\ \mu s$ with the proposed 1D-XLSA model to $t = 69\ \mu s$ for the 2D-XLSA

model. During this stage, the normalized amplitude decreases, as displayed in Fig. 7 a). Later, the growth rate remains always positive and the corresponding amplitude of the plastic strain perturbation is strictly increasing. Only for $t > 150\ \mu s$, growth rates are coinciding for both models and all initial conditions. An interesting outcome of the paper is to highlight how the way multiaxiality effects are introduced in the model affects the perturbation evolution for large wavenumbers. This is in agreement with Fressengeas and Molinari (1994).

Fig.8 displays the through-thickness variation of the stream function $\hat{\psi}^{2D-XLSA}(Y,t)$ computed by the 2D-XLSA model at a) $t = 125\ \mu s$ and b) $t = 200\ \mu s$. The two wavenumbers $\gamma_1 = 0.82/h_0^b$ and $\gamma_2 = 2.5/h_0^b$ are considered. Only the initial condition $IC2$ is adopted as it generates an initial fluctuation of the plastic strain perturbation in the plate thickness. At $t = 125\ \mu s$, the spatial variation in the Y direction of the stream function is non-linear, leading to a heterogeneous perturbation of the plastic deformation in the thickness of the plate. Therefore, difference between the 1D-XLSA and 2D-XLSA can be expected. At $t = 200\ \mu s$ *i.e.* in the late deformation stage, the spatial variation of the stream function amplitude becomes almost linear for both wavenumbers. Thus, the 2D-XLSA model provides results similar to those obtained with the proposed 1D model in terms of growth rate, see Fig.7b).

To provide a measure of the linearity of the solution at a given time, a polynomial interpolation of function $\hat{\psi}^{2D-XLSA}$ is performed: $\hat{\psi}^{2D-XLSA}(Y,t) = \sum_{n=0}^{\infty} q_{2n+1}(t) Y^{2n+1}$. Note that all coefficients related to an even order are null as the function is antisymmetric with respect to Y so as to be representative of necking mode. q_1 is the coefficient in the polynomial expansion representative of the linear shape of $\hat{\psi}^{2D-XLSA}$. Fig.9 displays the absolute value of the normalized coefficient $\frac{q_{2n+1}}{q_1}$ for n in the range $[0,7]$ at different times a) $t = 125\ \mu s$, b) $t = 200\ \mu s$. Two wavenumbers $\gamma_1 = 0.82/h_0^b$ and $\gamma_2 = 2.5/h_0^b$ are considered. With the initial condition $IC2$, it is found (results not presented here) that q_3 is the dominant coefficient at $t = 0$ with $q_3 \approx 3q_1$. At $t = 125\ \mu s$, Fig9a) shows that ratios $|q_{2n+1}/q_1|$ have been reduced for $n \geq 1$ meaning that the stream function amplitude is less non-linear. This is particularly visible for the perturbation with the small wavenumber γ_1 for which the coefficient q_1 is the dominant one. In other words, for this small wavenumber, the time duration when the effect of the modeling of multiaxiality and of the influence of the initial condition are significant, is short and the proposed 1D-XLSA model provides consistent results when compared to a multidimensional approach as the 2D-XLSA method. In the early deformation process, for the perturbation mode of large wavenumber γ_2, the stream function remains highly non-linear at $t = 125\ \mu s$, meaning that the perturbed plastic strain presents a strong fluctuation inside the plate thickness. Therefore, discrepancies in terms of amplitude and growth rate are expected, as observed in the early stage of the deformation process between the 2D-XLSA and the proposed 1D-XLSA models. At $t = 200\ \mu s$, it is seen in Fig.9b) that the stream function presents an almost linear fluctuation within the plate thickness for both wavenumbers as q_1 is clearly the dominant coefficient. Therefore, the proposed 1D-XLSA model and the 2D-XLSA approach capture similar growth rates, see Fig.6.

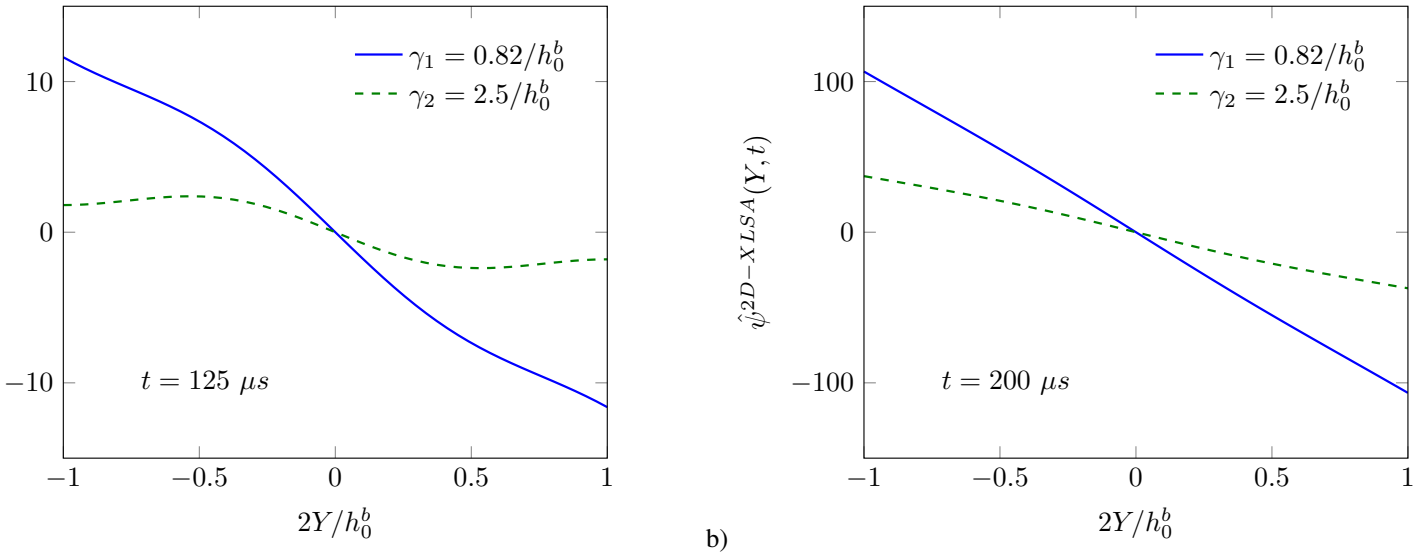

Figure 8: Spatial variation in the plate thickness of the stream function computed by the 2D-XLSA model for a) $t = 125\ \mu s$ and b) $t = 200\ \mu s$. Wavenumbers $\gamma_1 = 0.82/h_0^b$ and $\gamma_2 = 2.5/h_0^b$ are considered. Initial condition $IC2$ is used, see Fig.5. The material is thermoviscoplastic, with a powerlaw flow stress, see Eq.(20). Material parameters are listed in Table 1. The nominal strain rate is $\dot{\varepsilon}_0 = 2300\ s^{-1}$. Initial thickness is $h_0^b = 2.4\ mm$. Initial amplitude of the thickness perturbation is $\hat{h}_0 = 8\ \mu m$.

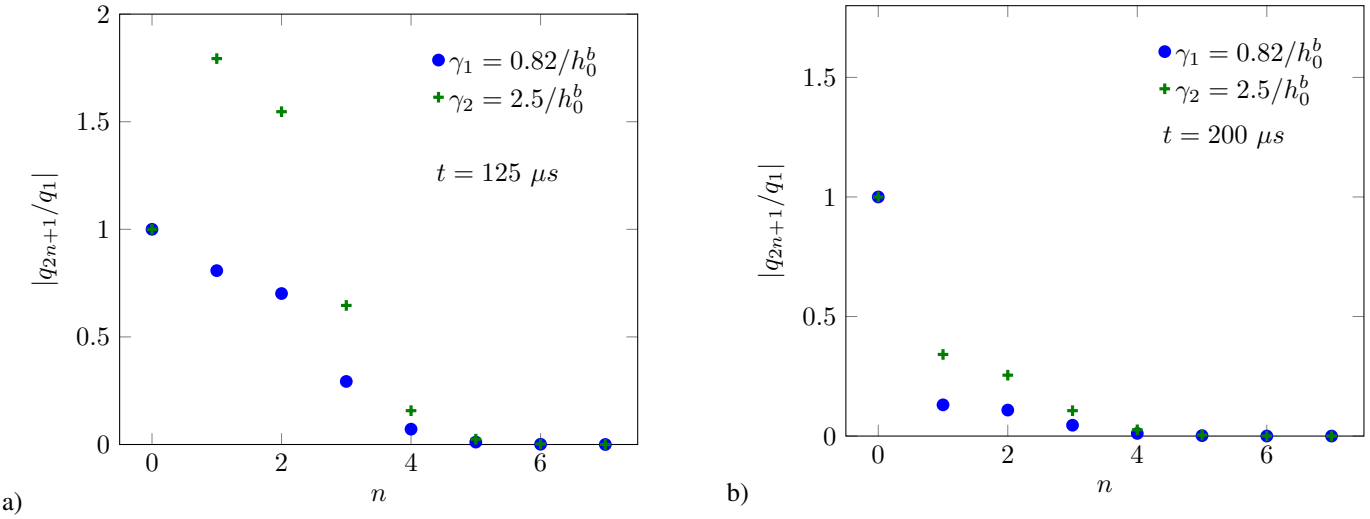

Figure 9: Values of the normalized coefficients $|\frac{q_{2n+1}}{q_1}|$ of the polynomial interpolation of $\hat{\psi}^{2D-XLSA}$ for n in the range $[0, 7]$. Interpolation is performed at a) $t = 125\ \mu s$ and b) $t = 200\ \mu s$. Two perturbation modes with wavenumber $\gamma_1 = 0.82/h_0^b$ and $\gamma_2 = 2.5/h_0^b$ are considered. Initial condition $IC2$ of Fig.5 is selected. The material is thermoviscoplastic, with a powerlaw flow stress, see Eq.(20). Material parameters are listed in Table 1. The nominal strain rate is $\dot{\varepsilon}_0 = 2300\ s^{-1}$. Initial thickness is $h_0^b = 2.4\ mm$. Initial amplitude of the thickness perturbation is $\hat{h}_0 = 8\ \mu m$.

4 Conclusion

A new linear stability analysis of a plate under plane strain loading is proposed to model multiple necking. A one-dimensional framework is used and multiaxiality of the stress field within the neck region is taken into account with a Bridgman correction factor. Contrary to models in the literature, except in Xavier et al. (2020), the assumption of exponential growth of the perturbation, only valid when the time scale separation prevails, is no longer used. The

thermo-mechanical problem is analyzed which leads finally to a system of two time differential equations coupling a mechanical perturbation and a thermal perturbation. The theory is exemplified by considering the stretching of a plate made of a thermo-viscoplastic material with strain hardening.

The importance of the modeling of multiaxiality and the role of the initial material configuration have been addressed. Indeed, while in the proposed 1D model the Bridgman correction factor is used, the 2D-XLSA model of Xavier et al. (2020) for which the stress field within the plate is really multi-dimensional, is also considered. It is shown that for perturbations with a large wavenumber, a discrepancy in amplitude is observed mainly due to difference in growth rates at the beginning of the stretching. For perturbations with a small wavenumber, both approaches provide similar amplitude evolution. It is therefore seen that the 1D-XLSA framework provides consistent results when compared to the 2D-XLSA model. It could be also of interest to perform an extensive comparison for various constitutive material responses. Note that the 1D-XLSA model of the present work is much simpler when compared to 2D-XLSA (also from a numerical point of view).

One of the main features of the proposed model is that the evolution of the perturbation can be captured at any deformation stage (during stable or unstable flow). This capability appears as an important achievement when compared to 1D linear stability analyses of the literature. Indeed, classical linear stability analyses based on frozen coefficient theory (as often adopted in the literature) are usually used to analyze the deformation stage during unstable flow, *i.e.* when positive growth rate for the perturbation is encountered (often late in the deformation process). Thus, during stable flow, we have assumed in the CLSA that the perturbation is frozen (no amplitude evolution is assumed). It is clear that, it could be of interest to further analyze with the classical linear stability analysis the evolution of perturbations during stable flow.

Comparisons with results obtained with linear stability analysis based on the frozen coefficient theory are performed. While growth rates of the two models (1D-CLSA and 1D-XLSA) are similar in the late deformation stages, large differences in terms of amplitude are found due to discrepancies inherited from the early deformation stage. This finding is valid for perturbations with any wavenumber. In addition, various initial conditions can be treated with the 1D-XLSA approach, while up to now, the 1D-CLSA method was not considering this possibility.

In a future work, finite element calculations will be conducted to compare predictions in terms of amplitude and spacing of necks. The goal will be to investigate how the 1D-XLSA model can help in predicting fragmentation of structural elements.

A 1D Linear stability analysis with frozen coefficient assumption

The governing equations for the perturbed quantities are given by the set (15) in which the initial conditions δh_0 and $\delta\varepsilon_p^0$ are not considered, see Zhou et al. (2006) or Zaera et al. (2015). In the frozen coefficient theory, perturbations are searched under the form $\delta G(X,t) = \hat{G}^0 cos(\gamma X)\exp(\eta t)$ with η the growth rate of the perturbation and $\hat{G}^0$ an amplitude factor, while δv is searched as $\delta v(X,t) = \hat{v}^0 sin(\gamma X)\exp(\eta t)$. When adopting the frozen coefficient theory, it is assumed that the time scale associated with the evolution of the perturbation is much smaller than the one associated to the homogeneous solution.

At each time t of the deformation process, a perturbation is superimposed to the background homogeneous solution. So, the expression of the perturbed quantities are substituted in the set of equations (15). After some rearrangement, and by selecting the perturbed plastic strain and the perturbed temperature as the two main variables:

$\delta\varepsilon_p(X,t) = \hat{\varepsilon}_p^0 cos(\gamma X)\exp(\eta t)$ and $\delta T(X,t) = \hat{T}^0 cos(\gamma X)\exp(\eta t)$, one obtains from the set of Eqs (15):

$$\begin{aligned} &\left(a_1\eta^2 + a_2\eta + a_3\right)\hat{\varepsilon}_p^0 + a_4\hat{T}^0 = 0 \\ &\eta\hat{T}^0 = b_1\hat{T}^0 + b_2\eta\hat{\varepsilon}_p^0 + b_3\hat{\varepsilon}_p^0 \end{aligned} \tag{24}$$

Coefficients in Eq.(24) are the same as those provided in Eq.(17) The combination of the two relations (24) provides:

$$a_1\eta^2 + a_2\eta + a_3 + a_4\frac{b_2\eta + b_3}{\eta - b_1} = 0 \tag{25}$$

After simple manipulation, Eq.(25) leads to a third order polynomial equation whose solution is η. The largest positive root of Eq.(25) is usually adopted as the instantaneous growth rate of the perturbation. It is used to represent the time evolution of the perturbation when the Bridgman approximation is considered in the linear stability analysis, see Zhou et al. (2006), Rodríguez-Martínez et al. (2013a).

B 1D Linear stability analysis of ductile expanding ring

Fragmentation of rings has been widely discussed in the literature and studied analytically with the use of the linear stability analysis of the dynamic extension of a round bar, see Jeanclaude and Fressengeas (1997), Mercier and Molinari (2003), Zhou et al. (2006), El Maï et al. (2014), Rodríguez-Martínez et al. (2013a). We propose to use the method of the present paper to extend the work of Zhou et al. (2006) without considering the frozen coefficient theory. The linear stability analysis of a round bar, of initial cross-section A_0 ($A_0 = \pi r_0^2$) is developed through a Lagrangian 1D analysis. In the present approach, we investigate the possibility of having an initial imperfection for the radius. Therefore, it is assumed that r_0 is possibly evolving along the length of the bar: $r_0(X) = r_0^b + \delta r_0(X)$ and the average of the perturbation is zero : $< \delta r_0(X) >= 0$. At time $t = 0$, the bar is strained under uniform nominal strain-rate $\dot{\varepsilon}_0 = V_0/L_0$. V_0 is the constant traction velocity and L_0 the initial half-length of the bar.

The Lagrangian coordinate is X ($-L_0 \leq X \leq L_0$). At time t, we define the following quantities: x the Eulerian coordinate, v the longitudinal velocity, σ the true stress, $\varepsilon = \ln(\dfrac{\partial x}{\partial X})$ the true strain and $A = \pi r^2$ the current section. All those variables are only related to t and X. The multidimensional aspect of the stress field within the neck region is accounted for by replacing the true stress σ by an average stress complemented by the Bridgman correction factor $B(\Phi)$ defined in Bridgman (1952), see also Appendix C. Governing equations detailed in Zhou et al. (2006) are briefly recalled:

$$\begin{array}{llll} \rho_0 A_0\dfrac{\partial v}{\partial t} = \dfrac{\partial A\sigma}{\partial X} & \dfrac{\partial x}{\partial X} = e^{\varepsilon} & \dfrac{\partial v}{\partial X} = \dot{\varepsilon}e^{\varepsilon} & A = A_0 e^{-\varepsilon} \\ \sigma = \left(1 + \frac{1}{\Phi}\right)\ln(1+\Phi)\sigma_Y & \Phi = \frac{1}{2}r\dfrac{\partial^2 r}{\partial x^2} & \sigma_Y = \sigma_Y(\varepsilon_p, \dot{\varepsilon}_p, T) & \rho_0 C\dot{T} = \beta^{TQ}\sigma_Y\dot{\varepsilon}_p \\ & \varepsilon_p - \varepsilon_p^0 = \varepsilon & & \end{array} \tag{26}$$

with C the thermal capacity supposed constant, β^{TQ} the Taylor-Quinney coefficient, supposed constant, and ρ_0 the mass density. The material is assumed incompressible. ε_p^0 is a pre-strain parameter.

The homogeneous solution G^b, representative of the deformation mode without any imperfections defined from

Eqs (26) can be found in Zhou et al. (2006):

$$\begin{array}{ll} x^b = (1+\dot{\varepsilon}_0 t)X \quad \varepsilon^b = \ln(1+\dot{\varepsilon}_0 t) > 0 \quad \Phi^b = 0 \\ A^b = A_0^b e^{-\varepsilon^b} \qquad \dot{\varepsilon}_p^b = \dfrac{\dot{\varepsilon}_0}{1+\dot{\varepsilon}_0 t} \end{array} \tag{27}$$

where $A_0^b = \pi r_0^b$ is the initial cross-section, without imperfection.

In the 1D linear stability analysis of the literature, as in Zhou et al. (2006), at each time step, a perturbation is added to the homogeneous solution. With the present approach, the perturbation is introduced at the initial time and its evolution is deduced consistently:

$$\begin{array}{lll} v = v^b + \delta v & \varepsilon = \varepsilon^b + \delta\varepsilon & \varepsilon_p = {\varepsilon_p}^b + \delta\varepsilon_p \\ A = A^b + \delta A & \sigma = \sigma^b + \delta\sigma & \sigma_Y = {\sigma_Y}^b + \delta\sigma_Y \\ \dot{\varepsilon} = \dot{\varepsilon}^b + \delta\dot{\varepsilon} & \Phi = \Phi^b + \delta\Phi & T = T^b + \delta T \end{array} \tag{28}$$

Substitution of Eq.(28) in the governing equations (26) and using the homogeneous solution defined in Eqs (27) provide the governing equations for the perturbed fields:

$$\begin{array}{ll} \dfrac{\partial \delta v}{\partial X} = e^{\varepsilon^b}\left(\dot{\varepsilon}^b \delta\varepsilon + \delta\dot{\varepsilon}\right) & \delta A = -A^b\delta\varepsilon + \delta A_0 e^{-\varepsilon^b} \\ \delta\sigma = \delta\sigma_Y + \dfrac{1}{2}\sigma_Y^b \delta\Phi & \rho_0 A_0^b \dfrac{\partial \delta v}{\partial t} = A^b \dfrac{\partial \delta\sigma}{\partial X} + \sigma^b \dfrac{\partial \delta A}{\partial X} \\ \delta\Phi = \dfrac{\exp(-2\varepsilon^b)}{4\pi}\dfrac{\partial^2 \delta A}{\partial X^2} & \delta\varepsilon_p - \delta\varepsilon_p^0 = \delta\varepsilon \\ \delta\dot{\varepsilon}_p = \delta\dot{\varepsilon} & \delta\sigma_Y = \sigma^b_{Y,\varepsilon_p}\delta\varepsilon_p + \sigma^b_{Y,\dot{\varepsilon}_p}\delta\dot{\varepsilon}_p + \sigma^b_{Y,T}\delta T \\ \rho_0 C \delta\dot{T} = \beta^{TQ}(\dot{\varepsilon}_p^b \delta\sigma_Y + \sigma_Y^b \delta\dot{\varepsilon}_p) & \end{array} \tag{29}$$

with $\sigma^b_{Y,\omega}$ denoting the partial derivative of σ_Y^b with respect to the variable ω (ω being ε_p, $\dot{\varepsilon}_p$ or T).

As for the stretching of the plate developed in the main part of the paper, perturbation fields δG are searched of the form $\delta G = \cos(\gamma X)\hat{G}(\gamma, t)$ (except for the perturbation of the velocity whose form is $\delta v = \sin(\gamma X)\hat{v}(\gamma, t)$, see Eq.3) with $\gamma = \frac{k\pi}{L_0}$ being the longitudinal wavenumber of the perturbation. After adequate combination, the set of Eqs (29) simplifies into two ordinary differential equations coupling the main unknowns $\hat{\varepsilon}_p$ and $\hat{T}$:

$$c_1\ddot{\hat{\varepsilon}}_p + c_2\dot{\hat{\varepsilon}}_p + c_3\hat{\varepsilon}_p + c_4\hat{T} = f_0 \qquad \dot{\hat{T}} = d_1\hat{T} + d_2\dot{\hat{\varepsilon}}_p + d_3\hat{\varepsilon}_p \tag{30}$$

The coefficients c_i and d_i in Eq.(30) are only time dependent, related to the homogeneous solution:

$$\begin{array}{ll} c_1(t) = \rho_0(1+\dot{\varepsilon}_0 t) & c_3(t) = \dfrac{\sigma_Y^b {A_0}^b \gamma^4}{8\pi(1+\dot{\varepsilon}_0 t)^4} + \dfrac{\sigma^b_{Y,\varepsilon_p}\gamma^2}{1+\dot{\varepsilon}_0 t} - \dfrac{\sigma_Y^b\gamma^2}{1+\dot{\varepsilon}_0 t} \\ c_2(t) = 2\rho_0\dot{\varepsilon}_0 + \dfrac{\gamma^2\sigma^b_{Y,\dot{\varepsilon}_p}}{1+\dot{\varepsilon}_0 t} & c_4(t) = \dfrac{\gamma^2\sigma^b_{Y,T}}{1+\dot{\varepsilon}_0 t} \\ d_1(t) = \beta^{TQ}\dfrac{\dot{\varepsilon}_0}{\rho_0 C(1+\dot{\varepsilon}_0 t)}\sigma^b_{Y,T} & d_3(t) = \beta^{TQ}\dfrac{\dot{\varepsilon}_0}{\rho_0 C(1+\dot{\varepsilon}_0 t)}\sigma^b_{Y,\varepsilon_p} \\ d_2(t) = \dfrac{\beta^{TQ}}{\rho_0 C}\left(\dfrac{\dot{\varepsilon}_0}{1+\dot{\varepsilon}_0 t}\sigma^b_{Y,\dot{\varepsilon}_p} + \sigma_Y^b\right) & \end{array} \tag{31}$$

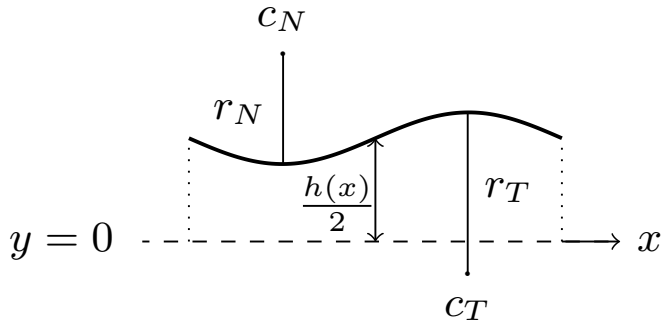

Figure 10: Schematic representation of the plate during deformation. The thickness profile is non-uniform.

f_0 is a time dependent coefficient that depends on the prescribed values of the amplitude $\hat{A}_0$ of the perturbation of the initial cross-section and the amplitude $\hat{\varepsilon}_p^0$ of the perturbation of the pre-strain parameter:

$$f_0 = -\left(\hat{\varepsilon}_p^0 + \frac{\hat{A}_0}{A_0^b}\right)\left[\frac{\gamma^2\sigma_Y^b}{(1+\dot{\varepsilon}_0 t)} - \frac{A_0^b\gamma^4\sigma_Y^b}{8\pi(1+\dot{\varepsilon}_0 t)^4}\right] \tag{32}$$

The system (30) has to be completed with initial conditions on $\hat{\varepsilon}_p(t=0)$, $\dot{\hat{\varepsilon}}_p(t=0)=0$ (since initial uniform strain rate is prescribed) and $\hat{T}(t=0)$. As for plane strain, when the frozen coefficient theory is adopted, the system (29), in which initial conditions $\delta\varepsilon_p^0$ and δA_0 are neglected, leads to a third order polynomial equation for the growth rate η. This equation can be found elsewhere, Zhou et al. (2006), Rodríguez-Martínez et al. (2013b), Rodríguez-Martínez et al. (2013a) or Vaz-Romero et al. (2017).

C Bridgman correction factor calculation

In this appendix, the expression of the Bridgman correction factor for plane strain conditions is briefly discussed, see Bridgman (1952) for more details.

Let us consider a half-plate with a non-uniform thickness $h(x)$, see Fig.10. The radius of curvature in the neck region is $r_N > 0$ while in the area where the plate is thicker than in the neck region, the surface profile is concave with a radius of curvature $r_T < 0$.

In the original paper of Bridgman (1952), a simplified analysis of the stress field at the neck has been proposed. From geometrical considerations on the shape of the neck region and of the isostatic lines (assuming a circle shape), the author found that the longitudinal stress at the neck is fluctuating in the cross-section according to the following expression:

$$\sigma(x) = 2\frac{\sigma_Y}{\sqrt{3}}\left[1 + \ln\left(1 + \frac{1}{4}\frac{h}{r_N}\left(1 - 4\frac{y^2}{h^2}\right)\right)\right] \tag{33}$$

with σ_Y being the flow stress.

Noticing that $\Phi = \frac{h}{4r_N}$, and by integration along the thickness of the plate at the neck, the expression of the

Bridgman correction factor is obtained as in Bridgman (1952):

$$\begin{aligned} B(\Phi) &= \frac{2}{h}\int_0^{\frac{h}{2}} (\left[1+\ln\left(1+\frac{1}{4}\frac{h}{r_N}\left(1-4\frac{y^2}{h^2}\right)\right)\right])dy \\ &= \sqrt{1+\frac{1}{\Phi}}\ln\left(1+2\Phi+2\sqrt{\Phi(1+\Phi)}\right)-1 \end{aligned} \tag{34}$$

The expression is valid for $\Phi > 0$. Thus, the Bridgman correction factor obtained in Eq.(34) for plane strain cannot be used when the profile is concave. Let us analyse now the stress field where the plate is thicker than in the neck region, labelled T in Fig. 10. The center of curvature of the external contour c_T is located on the other side of the axis of the plate. The radius of curvature is $r_T < 0$. By applying the same strategy as in Bridgman (1952) for the region where the plate is locally the thickest, one can easily show that the expression for the longitudinal stress is still given by Eq.(33), replacing r_N by r_T. Note that for the concave case, the parameter $\Phi = \frac{h}{4r_T}$ is negative. By integration as in Eq. (34), the novel expression of the Bridgman correction factor in the concave region where the plate is the thickest is:

$$B(\Phi) = \left[2\sqrt{-1-\frac{1}{\Phi}}\arctan\left(\frac{1}{\sqrt{-1-\frac{1}{\Phi}}}\right)-1\right] \tag{35}$$

In the present paper, for limited sine perturbation of the plate thickness, one has $r_N >> h$ and $-r_T >> h$. As a consequence, Φ remains close to zero. The Taylor expansion of Eqs (34) and (35) leads to the expression (11):

$$B(\Phi) = 1 + \frac{2\Phi}{3} + o(\Phi^2) \tag{36}$$

The last relation is valid at the neck and in the area where the plate is thicker than in the neck region. In the present paper, for limited amplitude of the perturbation, we assume that the formula (36) is extended by continuity so that the Taylor expansion of the Bridgman correction factor given by Eq. (36) is adopted for the entire plate, see for instance Zhou et al. (2006).

References

Audoly, B., Hutchinson, J. W., 2016. Analysis of necking based on a one-dimensional model. Journal of the Mechanics and Physics of Solids 97, 68 – 91.

Audoly, B., Hutchinson, J. W., 2019. One-dimensional modeling of necking in rate-dependent materials. Journal of the Mechanics and Physics of Solids 123, 149 – 171.

Bridgman, P. W., 1952. Studies in large plastic flow and fracture. McGraw-Hill Book Company, INC.

El Maï, S., 2014. Etude du développement des instabilités dans un anneau en expansion dynamique. Ph.d. thesis, Université de Lorraine, École doctorale EMMA, France.

El Maï, S., Mercier, S., Petit, J., Molinari, A., 2014. An extension of the linear stability analysis for the prediction of multiple necking during dynamic extension of round bar. International Journal of Solids and Structures 51, 3491–3507.

Fressengeas, C., Molinari, A., 1985. Inertia and thermal effects on the localization of plastic flow. Acta Metall. 33, 387–396.

Fressengeas, C., Molinari, A., 1994. Fragmentation of rapidly stretching sheets. Eur. J. Mech. A/Solids 13, 251–268.

Fyfe, I. M., Rajendran, A. M., 1980. Dynamic pre-strain and inertia effects on the fracture of metals. J. Mech. Phys. Solids 28, 17–26.

Goto, D. M., Becker, R., Orzechowski, T. J., Springer, H. K., Sunwoo, A., Syn, C., 2008. Investigation of the fracture and fragmentation of explosively driven rings and cylinders. Int. J. Impact. Eng. 35, 1547–1556.

Grady, D. E., 1981. Fragmentation of solids under impulsive stress loading. J. Geophys. Res. B2 86, 1047–1054.

Hill, R., Hutchinson, J. W., 1975. Bifurcation phenomena in the plane tension test. J. Mech. Phys. Solids 23, 239–264.

Hutchinson, J. W., Neale, K. W., 1977. Influence of strain rate sensitivity on necking under uniaxial tension. Acta Metall. 25, 839–846.

Jacques, N., 2020. An analytical model for necking strains in stretched plates under dynamic biaxial loading. International Journal of Solids and Structures 200-201, 198 – 212.

Jeanclaude, V., Fressengeas, C., 1997. Dynamic necking of rods at high strain rates. J. Phys. IV Colloque C3 7, 699–704.

Jouve, D., 2010. Etude analytique de l'instabilité plastique de striction pour une plaque sollicitée en traction biaxiale. Ph.d. thesis, Ecole Polytechnique, France.

Jouve, D., 2013. Analytic study of plastic necking instabilities during plane tension tests. European Journal of Mechanics A/Solids 39, 180–196.

Jouve, D., 2015. Analytic study of the onset of plastic necking instabilities during biaxial tension tests on metallic plates. European Journal of Mechanics A/Solids 50, 59–69.

Llorca, F., Juanicotena, A., 1997. Expanding ring test: numerical simulation - application to the analysis of experimental data. J. PHYS IV FRANCE 7 3, 235–240.

Longère, P., Dragon, A., 2008. Evaluation of the inelastic heat fraction in the context of microstructure-supported dynamic plasticity modelling. International Journal of Impact Engineering 35 (9), 992–999.

Mason, J., Rosakis, A., Ravichandran, G., 1994. On the strain and strain rate dependence of the fraction of plastic work converted to heat: an experimental study using high speed infrared detectors and the kolsky bar. Mechanics of Materials 17 (2-3), 135–145.

Mercier, S., Granier, N., Molinari, A., Llorca, F., Buy, F., 2010. Multiple necking during the dynamic expansion of hemispherical metallic shells, from experiments to modelling. J. Mech. Phys. Sol. 58 (7), 955–982.

Mercier, S., Molinari, A., 2003. Predictions of bifurcation and instabilities during dynamic extension. Int. J. Solids Struct. 40, 1995–2016.

Mercier, S., Molinari, A., 2004. Analysis of multiple necking in rings under rapid radial expansion. Int. J. Impact Eng. 30, 403–419.

Mott, N. F., 1947. Fragmentation of shell cases. In: Proceedings of The Royal Society. Series A. pp. 300–308.

Niordson, F. I., 1965. A unit for testing materials at high strain rates. Exp. Mech. 5, 29–32.

Olive, F., Nicaud, A., Marilleau, J., Loichot, R., 1979. Rupture behaviour of metals in explosive expansion. Inst. Phys. Conf. Ser. 47, 242–251.

Petit, J., Jeanclaude, V., Fressengeas, C., 2005. Breakup of copper shaped-charge jets: Experiments, numerical simulations, and analytical modeling. J. Appl. Physics 98, 123521.

Ravi-Chandar, K., Triantafyllidis, N., 2015. Dynamic stability of a bar under high loading rate: Response to local perturbations. International Journal of Solids and Structures 58, 301–308.

Rittel, D., 1999. On the conversion of plastic work to heat during high strain rate deformation of glassy polymers. Mechanics of Materials 31 (2), 131–139.

Rodríguez-Martínez, J. A., Vadillo, G., Fernández-Sáez, J., Molinari, A., 2013b. Identification of the critical wavelength responsible for the fragmentation of ductile rings expanding at very high strain rates. Journal of the Mechanics and Physics of Solids 61, 1357–1376.

Rodríguez-Martínez, J. A., Vadillo, G., Zaera, R., Fernández-Sáez, J., 2013a. On the complete extinction of selected imperfection wavelengths in dynamically expanded ductile rings. Mechanics of Materials 60, 107–120.

Shenoy, V. B., Freund, L. B., 1999. Necking bifurcations during high strain rate extension. J. Mech. Phys. Solids 47, 2209–2233.

Stainier, L., Ortiz, M., 2010. Study and validation of a variational theory of thermo-mechanical coupling in finite visco-plasticity. International Journal of Solids and Structures 47 (5), 705–715.

Vaz-Romero, A., Rodriguez-Martinez, J. A., Mercier, S., Molinari, A., 2017. Multiple necking pattern in nonlinear elastic bars subjected to dynamic stretching: The role of defects and inertia. International Journal of Solids and Structures 125, 232 – 243.

Wesenberg, D., Sagartz, M., 1977. Dynamic fracture of 6061-T6 aluminium cylinders. J. Appl. Mech. 44, 643–646.

Xavier, M., Czarnota, C., Jouve, D., Mercier, S., Dequiedt, J., Molinari, A., 2020. Extension of linear stability analysis for the dynamic stretching of plates: Spatio-temporal evolution of the perturbation. European Journal of Mechanics-A/Solids 79, 103860.

Zaera, R., Rodríguez-Martínez, J. A., Vadillo, G., Fernández-Sáez, J., Molinari, A., 2015. Collective behavior and spacing of necks in ductile plates subjected to dynamic biaxial loading. Journal of the Mechanics and Physics of Solids 85, 245–269.

Zhang, H., Ravi-Chandar, K., 2006. On the dynamics of necking and fragmentation- I. Real-time and post-mortem observations in Al 6061-O. Int. J. Fract. 142, 183–217.

Zhou, F., Molinari, J. F., Ramesh, K. T., 2006. An elastic-visco-plastic analysis of ductile expanding ring. Int. J. Impact Eng. 33, 880–891.